CALISTO: A cryogenic far-infrared/submillimeter observatory - art. no. 66870P

Article *in* Proceedings of SPIE - The International Society for Optical Engineering · September 2007

Impact Factor: 0.2 · DOI: 10.1117/12.731049

CALISTO: A Cryogenic Far-Infrared/Submillimeter Observatory

P. F. Goldsmith, C.M. Bradford, M. Dragovan, B. Khayatian, K. Huffenberger, I. J.O'Dwyer, K. Górski, H. W. Yorke, J. Zmuidzinas, C. Paine, C. Satter, & R. Lee

Jet Propulsion Laboratory, California Institute of Technology, Pasadena CA 91109

ABSTRACT

We present a design for a cryogenically cooled large aperture telescope for far–infrared astronomy in the wavength range 30 μm to 300 μm. The Cryogenic Aperture Large Infrared Space Telescope Observatory, or *CALISTO*, is based on an off–axis Gregorian telesocope having a 4 m by 6 m primary reflector. This can be launched using an Atlas V 511, with the only optical deployment required being a simple hinged rotation of the secondary reflector. The off–axis design, which includes a cold stop, offers exceptionally good performance in terms of high efficiency and minimum coupling of radiation incident from angles far off the direction of maximum response. This means that strong astronomical sources, such as the Milky Way and zodiacal dust in the plane of the solar system, add very little to the background. The entire optical system is cooled to 4 K to make its emission less than even this low level of astronomical emission. Assuming that detector technology can be improved to the point where detector noise is less than that of the astronomical background, we anticipate unprecedented low values of system noise equivalent power, in the vicinity of 10^{-19} $WHz^{-0.5}$, through *CALISTO*'s operating range. This will enable a variety of new astronomical investigations ranging from studies of objects in the outer solar system to tracing the evolution of galaxies in the universe throughout cosmic time.

Keywords: Far–Infrared, Submillimeter, Space Observatory, Crogenic Telescope, Background–limited Sensitivity

1. INTRODUCTION

The stunning success of the *Spitzer* infrared space telescope has generated enormous excitement in the astronomical community about observations at longer–than–visible wavelengths. Some highlights are summarized by Werner *et al.*[1] The astronomical reasons for continuing observations in the far–infrared/submillimeter wavelenth range are many, but a few of the most prominent are

- The blackbody curves for emission from dust and gas heated by newly formed stars peaks in the 30 μm to 100 μm range and consequently this is the prime spectral region for studying the process of star formation in the Milky Way
- This spectral range is redshifted to systematically longer wavelengths for distant galaxies in the universe, so that the 100 μm to 300 μm range is ideally suited for studying the evolution of galaxies throughout cosmic time. With *CALISTO* we will have an extremely sensitive tool for probing how star formation and chemical enrichment have varied over billions of years.
- The pure rotational lines of H_2, the most common molecule in the universe, are in the wavelength range of a few to 28 μm, and when redshifted, these demand high sensitivity systems covering the 30 μm to few hundred μm range to observe this key constituent of galaxies and stars throughout the universe.
- The disks associated with the formation of stellar systems as well as the debris disks left over from the formation of planets have their emission peaks in this spectral range, as do objects in the outer parts of our own solar system. Study of all of these will greatly improve our understanding of how planetary systems form.

Send correspondence to Paul.F.Goldsmith@jpl.nasa.gov

UV/Optical/IR Space Telescopes: Innovative Technologies and Concepts III
edited by Howard A. MacEwen, James B. Breckinridge
Proc. of SPIE Vol. 6687, 66870P, (2007) · 0277-786X/07/$18 · doi: 10.1117/12.731049

The success of *Spitzer* built upon earlier infrared astronomy missions including the *Infrared Astronomy Satellite (IRAS)*, and the *Infrared Space Observatory (ISO)*. These missions advanced the state of the art in terms of sensitivity, spectral resolution, and sky coverage in the infrared, but were restricted to wavelengths shorter than 200 μm. While having cooled optical systems to maximize sensitivity, they had mirror diameters less than 1 m. In addition to *Spitzer* which has focused on relatively limited areas on the sky, the *Akari* satellite is carrying out large–area surveys in the infrared.

In the relatively near future, the *Herschel Space Observatory* will be launched (currently scheduled for August 2008). *Herschel* has three instruments covering the wavelength range from 1 mm to 60 μm, with spectral resolutions $\nu/\delta\nu$ as high as 10^6. The 3.5 m diameter reflector on *Herschel* will offer good angular resolution and it will have impressive sensitivity for the higher spectral resolution observations. The primary and secondary reflectors are cooled to only $\simeq 70\ K$, so that their emission will limit sensitivity for broadband observations.

The *Stratospheric Obsevatory for Infrared Astronomy (SOFIA)* will be starting observations within the next few years, and will give access to much of the spectral region blocked by atmospheric water vapor absorption. *SOFIA* will have a 2.5 m diameter mirror, but it will be at essentially room temperature, and the emission from the reflecting surfaces themselves will again be the limiting factor for broadband observations.

The *James Webb Space Telescope (JWST)* is scheduled to be launched in 2013. This facility will have dramatically improved performance at near–infrared wavelengths thanks to a 6 m diameter mirror and advanced detectors. Like *Herschel*, *JWST* will be launched to an L2 orbit and it is not envisioned that there will be any opportunity for instrument changeout. Thus, its long wavelength limit of 30 μm means that *JWST* will only explore the short wavelength portion of the infrared spectral range.

SPICA is an infrared mission that has been discused for launch in approximately a decade. It will have a 3.5 m diameter mirror as does *Herschel*, but cooled to 4 K, in order to reduce its thermal emission.

The best sources for current information on these projects are the appropriate web sites. Their number and diversity indicate that there remains an enormous amount of interest in long wavelength astronomy, and that we should consider what will be needed in the far–infrared (FIR), also sometimes referred to as the Submillimeter (Submm) spectral range. While definitions differ, we will adopt the pragmatic wavelength interval of 30 μm to 300 μm, as the "gap" which needs to be filled for very high sensitivity astronomy. This interval spans the longest wavelength that will be covered by *JWST* and the shortest wavelengths which can be observed from the ground by such facilities as the *Atacama Large Millimeter Array (ALMA)*, and the *Cornell Caltech Atacama Telescope (CCAT)*.

An earlier study had developed a concept for a future FIR/Submm facility, *SAFIR*, anacronym for *Single Aperture Far InfRared* observatory. *SAFIR* was based on a 10 m diameter primary reflector cooled to 4 K (Lester *et al.* 2005).[2] This offered impressive sensitivity, but the aperture size required petallization and on–orbit deployment. The gaps between the panels, and the blockage and scattering from the subreflector and support struts in this on–axis design all reduced antenna efficiency. More importantly, they produce significant scattering, and thus coupling to sources far from the telescope pointing direction. In the case of an ultra–low background instrument, which is necessary for maximum sensitivity, the strong emission from astronomical sources such as the plane of the Milky Way and the zodiacal emission from dust in our solar system can significantly degrade sensitivity.

These considerations, together with wanting to look for a lower cost approach for a next–generation FIR/Submm facility led us to the concept which we describe here. We call our mission *CALISTO*, an acronym for *Cryogenic Aperture Large Infrared Space Telescope Observatory*. Here we give details about the overall mission as well as the optical design presented previously.[3–5]

2. OPTICAL DESIGN

2.1 General Considerations

The design of the *CALISTO* optical system is driven by wanting to achieve maximum sensitivity over as much of the sky as possible. We are primarily addressing the following concerns.

1. We wish to achieve the maximum effective collecting area for the telescope. This requires a tradeoff of physical area and efficiency
2. In order to make this mission affordable, we wish to minimize deployment of critical optical elements
3. To maximize sensitivity, we envision cooling the entire telescope system to very low temperature
4. To ensure that this sensitivity is not compromised, we need to obtain a clean radiation pattern for the telescope. We thus have to minimize response far from the telescope pointing direction
5. We envision a suite of instruments which will exploit the capabilties of *CALISTO* over the wavelength range of 30 μm to 300 μm wavelength, and have a baseline of 10^4 diffraction–limited pixels at all wavelengths.

We have selected a primary reflector 4 m by 6 m in projected dimensions, as the largest size that can be accomodated in an Atlas V 511 without any deployment. This is a very important consideration for minimizing cost. This is evidently less physical area than, for example, the 10 m circular aperture envisioned by the previous *SAFIR Vision Mission Study*.[2] We partially compensate for the smaller physical area by a higher efficiency resulting from the unblocked aperture design.

The maximum angular resolution of the *CALISTO* telescope ranges from $12''$ at 300 μm wavelength to $1.2''$ at 30 μm. While not comparable to that of large optical telescopes or long–wavelength interferometers this is sufficiently high that many sources such as debris disks and nearby galaxies will be resolved. It also means that the confusion limit from extragalatic sources is reasonably low. Based on data obtained using *Spitzer*, the confusion limit for the 5 m diameter circular aperture representing the *CALISTO* beam is 5 μJy at 70 μm wavelength.

2.2 Limiting Sensivity

For a telescope in space, the system noise is the combination of the detector noise and the photon noise from the combination of unwanted emission (*e.g.* the reflector surfaces and from the astronomical input to the telescope). Of these three contributions, we can in principle reduce the detector noise by technological developments resulting in lower *Noise Equivalent Power* (NEP). We can control the unwanted emission by minimizing the emissivity ϵ, of any surface that couples to the detectors, and by reducing its temperature T.

For a single mode of the electromagnetic field in a bandwidth $d\nu$, the mean photon rate is $nd\nu$ and the mean power is $nh\nu d\nu$, where n is the photon occupation number. For a thermal source, $n = \epsilon[\exp(h\nu/kT) - 1]^{-1}$. Fluctuations in n result in an effective noise from the photon field, which is equivalent to a NEP given by

$$NEP = \sqrt{2(h\nu)^2 n(n+1)d\nu} \ , \tag{1}$$

as discussed in detail by Zmuidzinas (2003).[6] The different sources of noise add together as the root sum square of the NEP's of the detector, telescope, and background noise sources.

The premise of *CALISTO* is that we want to be limited by the astronomical background noise. This means that the detector noise and telescope noise must be less than that from the sky. The astronomical background is a combination of different sources which dominate at different wavelengths, as described by Benford *et al.* (2004).[7] The cosmic microwave background (a 2.7 K blackbody) is dominant at millimeter wavelengths, dust emission from the Galaxy is the strongest component in the 300 μm to 50 μm wavelength range, and dust in the solar system producing the zodiacal emission is strongest at shorter wavelengths. To assess the limiting sensitivity for *CALISTO*, we have taken the values at the North Eclipic Pole. The resulting values of the NEP for two different fractional bandwidths are shown in Fig. 1. These are very low values in terms of current state of the art technology for detectors, especially for the moderate resolution spectroscopic situation characterized by $\delta\nu/\nu = 0.001$. It will be a challenge to get detector NEP to be below these levels, but this is what is required to achieve astronomical background limited sensitivity.

The emission from the telescope must also be controlled to achieve the best sensitivity. In Fig. 2 we show the NEP that would results from three telescope temperatures, all assumed to be characterized by an emissivity of 5%. This value is the sum of the emissivity of all the surfaces (a minimum of two) so that it is not an

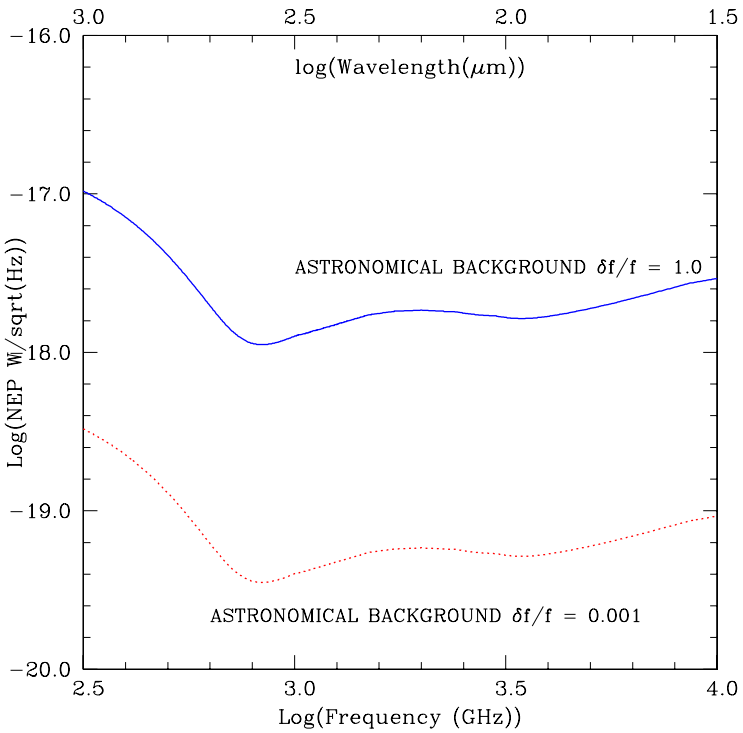

Figure 1. Limiting *Noise Equivalent Power* (*NEP*) from astronomical background at the North Ecliptic Pole. The upper curve is for a fractional bandwidth of 1.0 and the lower for fractional bandwidth of 0.001.

unreasonably pessimitic value. We see that for temperatures of 10 K or 20 K, the surface emission dominates the NEP throughout *CALISTO*'s operating range. Only for $T = 4.5$ K do we have the wavelength range $\lambda \leq 300$ μm dominated by the astronomical background. This sets the requirement that the temperature of the *CALISTO* optical system be no greater than 4.5 K.

2.3 System Configuration

The nominal optical design is an offset Gregorian system, with paraboloidal main reflector and ellipsoidal secondary reflector. The primary focal ratios are 0.67 and 1.0, and the secondary focal ratios are 3.0 and 4.5. A cross section of the optical system is shown in Fig. 3. The imaging qualities of the Gregorian system are relatively good. Using a ray tracing program, we have found that very minor changes in the surface shapes (changing the standard Gregorian to an aplanatic Gregorian having surfaces with different radii of curvature along orthogonal directions) enable diffraction–limited imaging over a field that easily includes 10^4 pixels at any wavelength between 30 μm and 300 μm. Detailed calculations of the response pattern of the telescope have been carried out using the nominal Gregorian configuration of a system with a 10 m diameter circular primary, and are discussed below.

3. TELESCOPE RADIATION PATTERNS

To analyze and compare performance of different designs, we have utilized the GRASP9 software package from TICRA software. We combine physical optics calculation for the main beam and close–in sidelobes with a Geometrical Optics and Geometrical Theory of Diffraction (GO/GTD) calculation for large angles (Goldsmith *et al.* 2006).[3] Calculations were carried out at a wavelength of 1 mm to minimze computational time. Selective checks have been made at a wavelength of 100 μm and show expected behavior in terms of scaling as a function of size divided by wavelength.

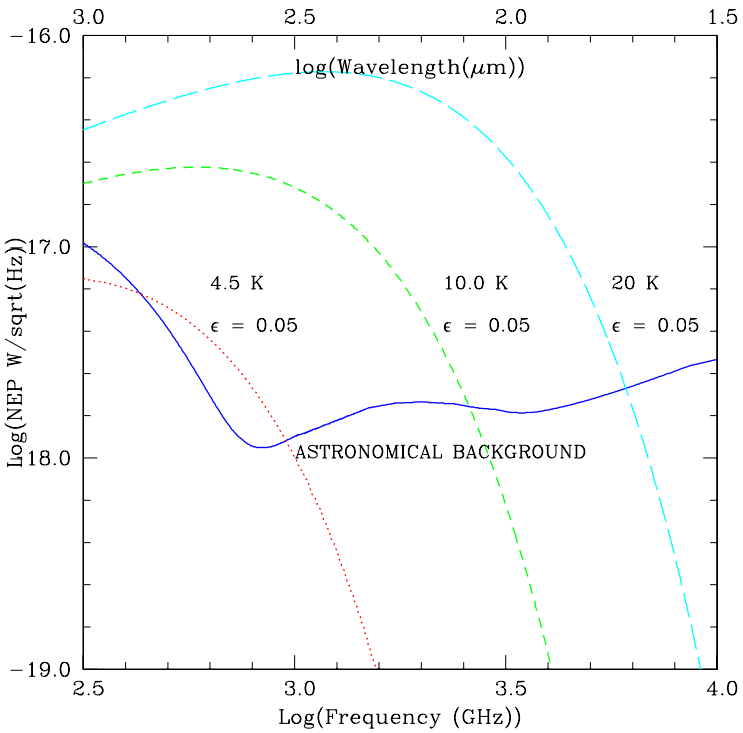

Figure 2. Limiting *Noise Equivalent Power* (*NEP*) from astronomical background at the North Ecliptic Pole compared to that resulting from an optical system having $\epsilon = 0.05$ at the three temperatures indicated. The fractional bandwidth $\delta f/f = 1$, but this does not affect the relative values of astronomical and telescopecontributions. Only for $T \leq 4.5K$ do we have the potential of astronomical background limited operation throughout the *CALISTO* wavelength range.

Our main interest here is to quantify the differences between symmetric (on–axis) designs and off–axis designs. We feel that the latter should have many inherent advantages especially for very low–background situations. In order to keep the comparison as clean as possible, we have in both cases analyzed designs with 10 m diameter primary reflectors. The first case consists of the symmetric design discussed in Lester *et al.* (2005)[2] and in Goldsmith *et al.* (2006).[3,4] The second case is an off–axis design having primary focal ratio $f/D = 0.67$ and secondary focal ratio 3.0, discuseed in Yorke *et al.* (2006).[5] The third case is the same as the second, but with the addition of a cold stop. This is a cooled termination for energy which would spill over past the edge of the secondary reflector. Given that the cold stop is cooled to 4 K, the power it emits which is coupled to the detector is very small. It has the major advantage that this potential coupling to the astronomical background is eliminated. As we will see this dramatically increases the fraction of the sky which is truly "low background".

In our previous paper, we showed that the aperture efficiency of the unblocked reflector is 0.80 for a Gaussian illumination with 12 dB edge taper.[3] This is to be compared with the aperture efficiency of 0.55 for the Vision Mission symmetric design. From this point of view, the unblocked 6 m by 4 m aperture has the same effective area as a 5.9 m diameter circular aperture. The cold stop shown in Fig. 3 does not change the aperture efficiency, but only terminates the spillover radiation at 4 K rather than allowing it to couple to the sky in an annular pattern offset from the main lobe of the telescope response.

The salient undesirable features of the response pattern of the first (on–axis) case are (1) the close–in sidelobes produced by the secondary reflector blockage, (2) the spillover past the secondary reflector, and (3) the threefold–symmetric large–angle pattern resulting from scattering from the three subreflector support struts.[3] These are illustrated in Fig. 4. The magnitude and angular distribution of the secondary blockage contribution depends on its size, which is largely dictated by the imaging field of view. For the Vision Mission *SAFIR* design, the subreflector diameter is 2 m. The angular size of its diffraction pattern is thus 5 times larger than the width of

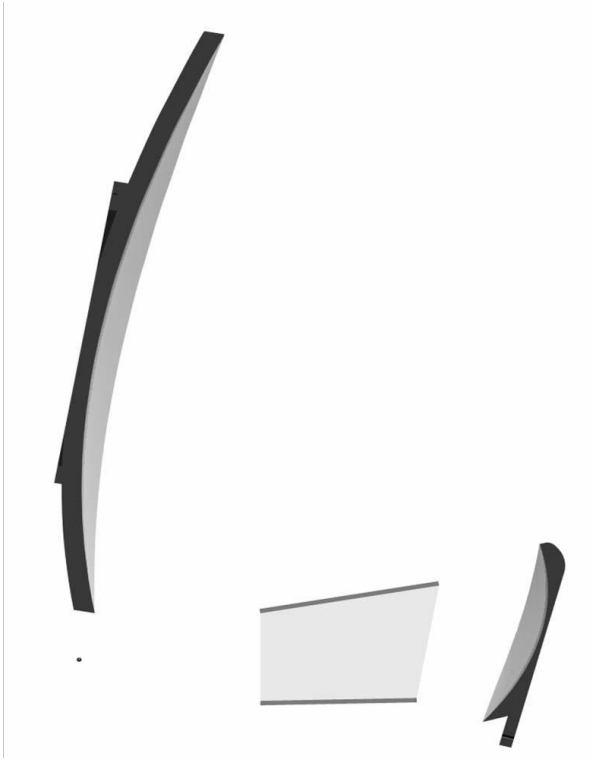

Figure 3. Cross section of CALISTO off–axis Gregorian optical system. The primary reflector is on the left, the secondary on the right, and the cold stop is the tapered cylindrical structure in between them. All these elements are cooled to 4 K. The Gregorian focal point is indicated by the dot below the primary reflector.

the main lobe of the telescope response pattern. There are many sidelobes, however, extending to singificantly larger angular distances, which at certain angles can reinforce the sidelobes from the primary reflector truncation.

The pattern of the radiation which spills past the edge of the secondary is an axially symmetric Gaussian with its central portion removed. The edge diffraction modifies this somewhat, but this contribution is nontheless strongest at an angle just greater than that defined by the edge of the secondary reflector as seen from the secondary focus. In the present case this is at 4° from maximum response. This spillover is unavoidable for the symmetric geometry, and amounts to approximately 5 percent of the energy coupled to the detectors. The strut scattering depends in detail on the geometry of the telescope, but for the Vision Mission *SAFIR* design, extends over an angular range out to 22° from the direction of maximum response. This is potentially the most harmful, as it can couple to radiation from an astronomical source in a quite different portion of the sky than is being observed with the main beam.

In the off–axis geometry we completely eliminate the blockage of the secondary and the scattering by the support struts. This is a great improvement, as indicated by the increase in the aperture efficiency given above. Elimination of blockage also reduces the response at large angles. The cleaner beam is certainly a great improvement over that of the symmetric consideration, but a problem that remains is the spillover past the subreflector boundary. This can be seen in Fig. 5. The spillover is at a fairly high level just outside the angular range subtended by the secondary reflector. It is also evidently displaced from the direction of maximum telescope response (at coordinates (0,0) in the Figure), due to the offset geometry. In order to remove the spillover past the secondary reflector we utilize a cold stop. This is an absorber, which is located between the secondary reflector and the secondary focus, in a region where there is an image of the primary reflector (the image plane is not perfectly defined because of the significant range in angles from different detectors). Geometrically, the cold stop absorbs all of the spillover, without changing the illumination of the telescope. In fact, the diffraction produced by the edge of the secondary does produce a ring–like feature in the overall radiation pattern, but this is at a

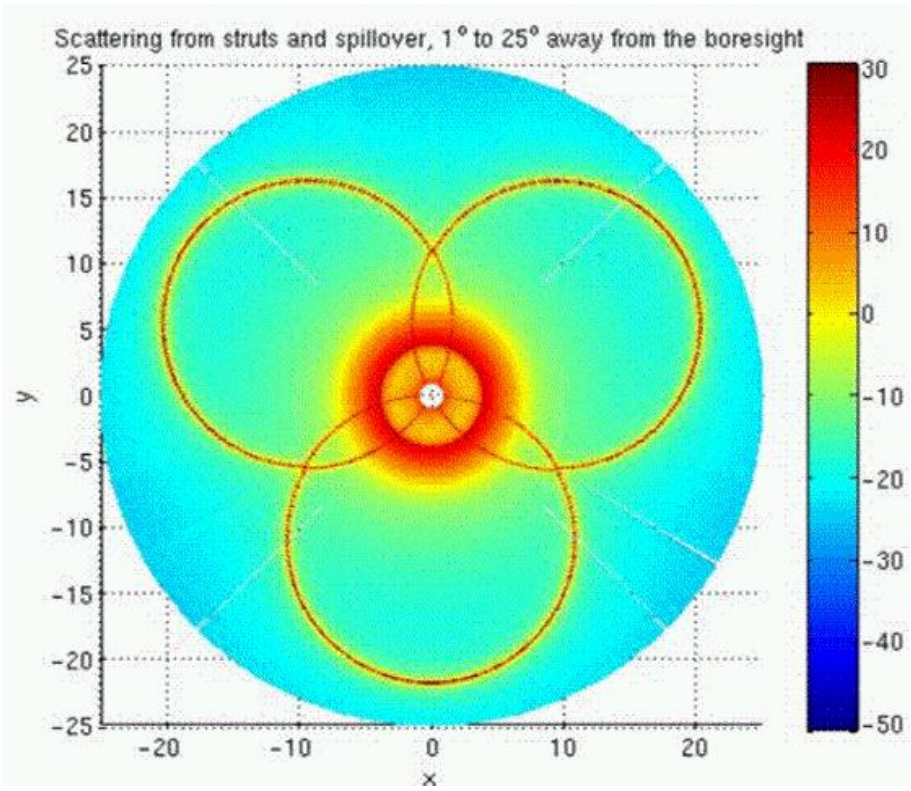

Figure 4. Response of the on–axis SAFIR design. The various contributions are indicated, with gain given by the color bar on the right (in decibels). The main lobe and close–in sidelobes have been supressed to emphasize the spillover around the secondary edge and the scattering from the secondary support struts.

much lower level than the geometrical spillover.

Elimination of the geometrical spillover results in a much lower fraction of the total power in the overall telescope radiation pattern being in the range outside the angle subtended by the secondary. We give results with and without the cold stop in Fig. 6. The two dimensional patterns have been integrated azimuthally around the main beam axis of symmetry to obtain these data.

We see a dramatic reduction, by more than an order of magnitude, in the power in the region between 3° and 40°, along with a substantial reduction in the power at larger angles. The power coupled to the cold stop, which is approximately 6% of the total, must be added to the third column. We note that there is approximately 2% of the power missing. We attribute this to the use of a "virtual feed" to generate the illumination of the primary reflector.[3] This feed has an ideal Gaussian pattern, rather than that which would be generated by reflection from the secondary reflector. While computationally efficient, this approach does introduce some error in the exact amplitude of the primary illumination which manifests itself as power "lost".

3.1 Coupling to Astronomical Background

To illustrate the dramatic difference between these optical designs, we have carried out a calculation which mimics a very important consideration for use of *CALISTO*. In it, we start with the astronomical background at 100 μm wavelength from the Milky Way. This is taken from the on–line data made available by Schlegel, Finkbeiner, & Davis (1998).[8] This includes the diffuse background measured by the *COBE* and *ISO* satellites. The contributions from the zodiacal foreground emission and from point sources have been removed. The computation was carried out using the technique described by Wandelt and Górski (2001).[9] In the following Figures we show the convolution of the telescope beam patterns, with the main lobe and near–in sidelobes excised, with the sky brightness at 100 μm. The purpose is to emphasize the contribution from the extended emission

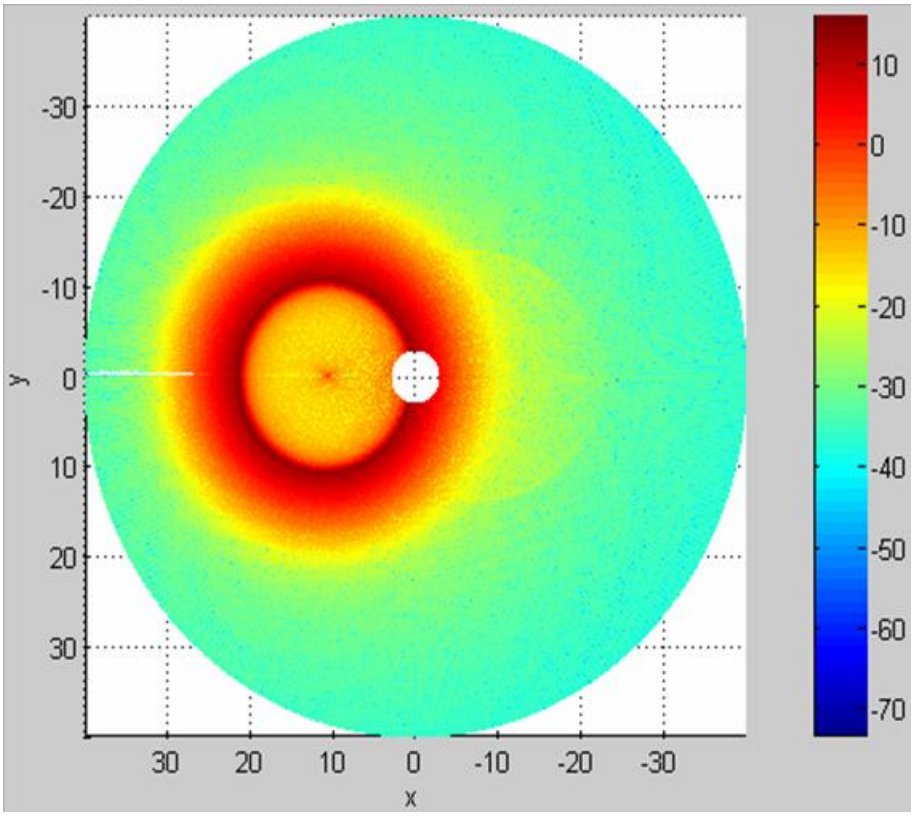

Figure 5. Radiation pattern of unblocked offset *CALISTO* telescope geometry. The main lobe and near–in diffraction sidelobes have been suppressed to emphasize the spillover past the secondary reflector. The angular range covered is $\pm 40^{\circ}$ in each axis. The scale at right gives the relative response in decibels.

Percentage of Integrated Power	Without Cold Stop	With Cold Stop
0 to 3 degrees	92.1	91.8
3 to 40 degrees	5.1	0.4
40 to 180 degrees	1.0	0.4

Figure 6. Percentages of integrated power in different angular regions with and without cold stop

as received by the far–out sidelobes of the radiation pattern. In each Figure the scale is the logarithm of the specific intensity in $MJy\ sr^{-1}$, or $10^{-20}Wm^{-2}Hz^{-1}sr^{-1}$. The scale is the same for all telescope configurations. The images are all in Mollweide Galactic projection, with the Galactic equator running horizontally across the middle of the image, and the Galatic North and South poles at top and bottom, respectively.

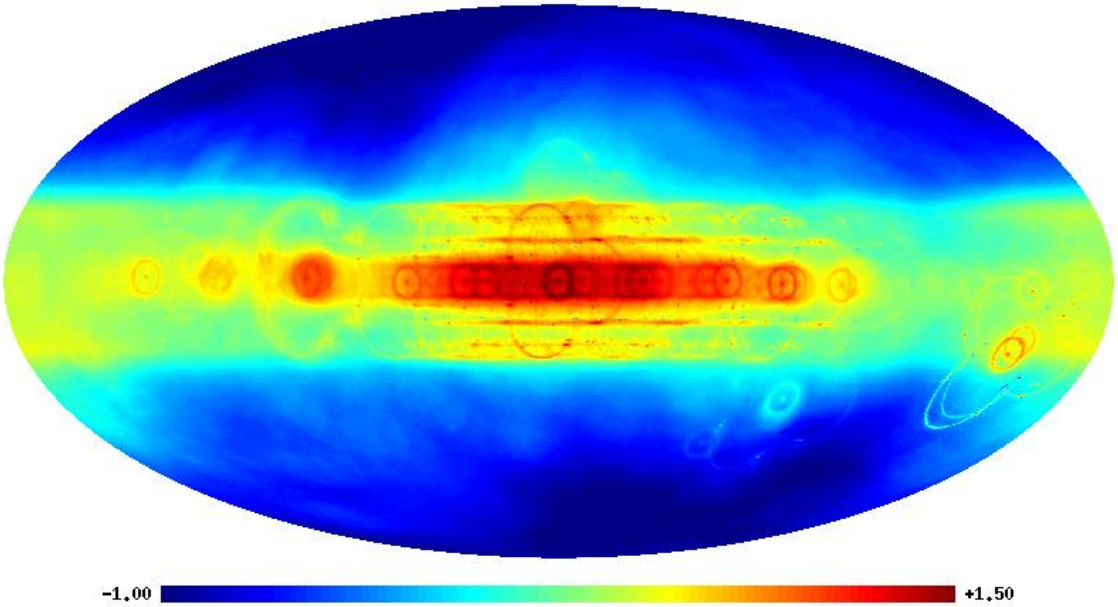

Figure 7. Sky brightness at 100 μm wavelength as measured with the on–axis (*SAFIR*–like) configuration. Every strong pointlike source produces a three-fold symmetric pattern from the large–angle scattering produced by the subreflector support struts. The response of the main beam and close–in primary reflector diffraction sidelobes has been supressed. The scale is $log_{10}(I_{100\mu m}/MJysr^{-1})$.

In Fig. 7 we see the effect of the secondary spillover and the secondary support scattering given in Fig. 4. The relatively high level of this pickup extends over a large portion of the solid angle of the sky.

In Fig. 8 we show the pattern for the off–axis *CALISTO* configuration. Recall that the calculations for the off–axis configurations are done with a circular 10 m aperture for most direct comparison with the on–axis results. We see in this Figure the significant improvement resulting from going to the off-axis configuration, but the secondary edge diffraction is still present, and results in the nearly circular pickup patterns around each strong pointlike source in the Galactic plane. Since this component of the telescope radiation pattern is offset with respect to the telescope axis, there is an optimium spacecraft roll angle for observing a given portion of the sky away from the plane. While there is a reduction in the fraction of the sky for which the unwanted pickup is strong, the spillover is still very prominent and makes the Galactic plane look much thicker than it really is.

The response of the *CALISTO* telescope with the cold stop is shown in Figs. 9 and 10. These show a dramatic improvement relative to the performance of the configurations previously presented. By choosing the optimum spacecraft roll angle, much of the sky can be observed with an additional background level due to unwanted pickup from the Galacic plane of $\leq 1\ MJysr^{-1}$ ($10^{-20}Wm^{-2}Hz^{-1}sr^{-1}$). This is an order of magnitude less than the "dark sky" value far from the plane, and thus indicates that we can achieve astronomical background limited operation over a large fraction of the sky, as far as the telescope design is concerned. The relatively diffuse low–level pickup is due to diffraction past the rim of the primary reflector. This, in principle, is circular, but the projection used to make these images together with the large angular size of this component of the telescope pattern result in the somewhat unobvious appearance here.

In reality, the astronomical background is more complex, and the different components have different angular distributions, as illustrated by Kelsall *et al.* (1991).[10] This only increases the importance of having a telescope

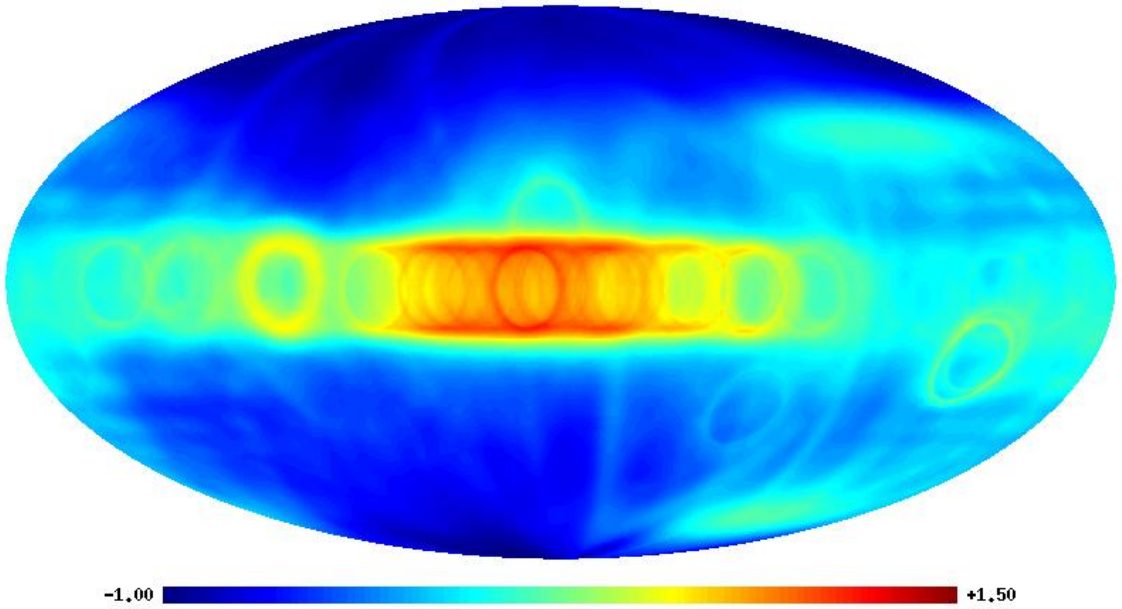

Figure 8. Sky brightness at 100 μm wavelength as measured with the off–axis *CALISTO* configuration. Note the elimination of the large–scale features seen in Fig. 7. The response of the main beam and close–in primary reflector diffraction sidelobes has been supressed. The scale is $log_{10}(I_{100\mu m}/MJysr^{-1})$.

response pattern with minimum pickup far from the direction of maximum response, in order that the largest fraction of the sky possible can be observed with high sensitivity.

4. SPACECRAFT DESGIN AND MISSION CONCEPT

A view of the overall spacecraft is shown in Fig. 11.

4.1 Cryogenic System Design

The design of the spacecraft is primarily driven by thermal considerations. A five layer V–groove sunshield is employed to assist in cooling the telescope. Current models indicate that three pulse tube coolers (2 operational, 1 redundant) provide 18 K precooling. Four Joule-Thomson systems are employed. Two provide cooling for the 4 K telescope and the topmost (furthest from the sun) sunshield. One J–T system cools the instrument environment, and one is used for 2 K instrument internal cooling. Additional sub–Kelvin coolers will be needed for the instruments, which are likely to be adiabatic demagnetization refrigerators (ADRs). These technologies are similar to what are being used for *JWST*.

Keeping the optics and detector systems at the required temperature necessitates having the spacecraft oriented so that the sunlight falls essentially normally on the sunshade. The sunshade dimensions are sized to allow a $\pm$ 15° inclination. With *CALISTO* in an L2 halo orbit, celestial objects located in a band defined by rotating the antenna pointing direction around the spacecraft–sun axis with a 30° width can be observed at a given time.

Some of the key *CALISTO* spacecraft and mission parameters are given in Fig.12.

4.2 Launch, Orbit, and Telescope

One of the key considerations for *CALISTO* is that any system deployment be as simple as possible. This immediately suggests that the primary not require any deployement as this is inevitably very complex and demanding in terms of precision. We have adopted an off–axis geometry which, in addition to offering much

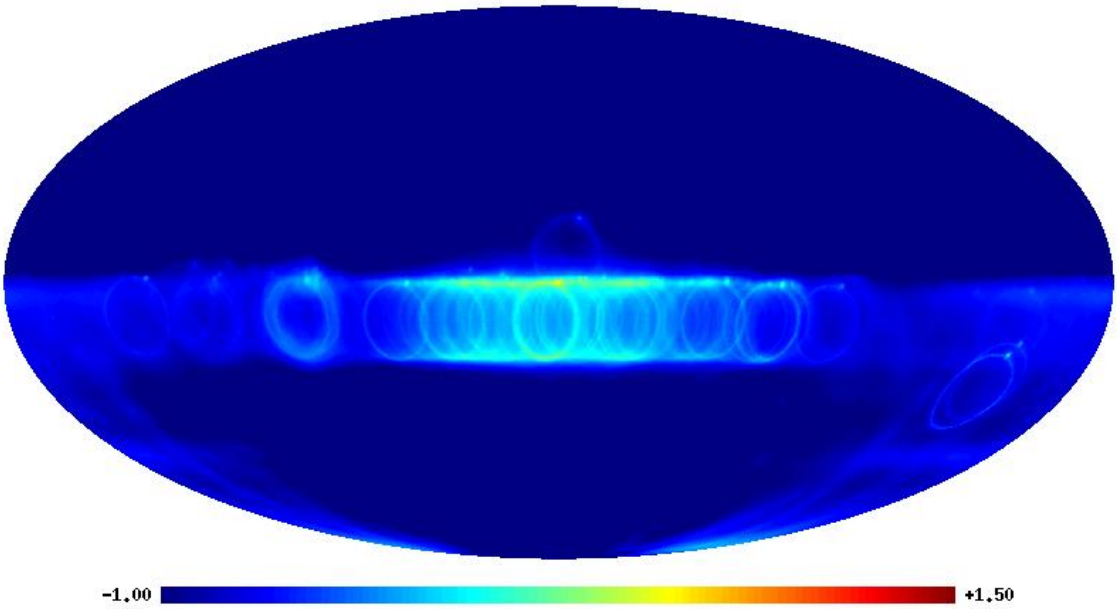

Figure 9. Sky brightness at 100 μm wavelength as measured with the off–axis *CALISTO* configuration including the cold stop. There remain relatively weak, circular features offset with respect to the direction of maximum response due to the secondary edge diffraction. These depend on the orientation of the spacecraft relative to the sky. The response of the main beam and close–in primary reflector diffraction sidelobes has been supressed. The scale is $log_{10}(I_{100\mu m}/MJysr^{-1})$.

improved optical performance as described in Section 2, also is extremely well–adapted to maximizing collecting area not requiring primary reflector deployment.

The ellipsoidal primary reflector is a good fit in the shroud of the Atlas V 511 launch vehicle. The V–groove thermal shields and solar panels are first deployed after launch. Subsequently, the *only* deployment of the telescope system is that of the cold stop and secondary reflector. This is a very simple deployment involving only a single hinged rotation to a final stop. The secondary reflector is supported on an actuated hexapod for focus and tip–tilt corrections, and this system can easily correct for any small errors in the deployment process as well. The off–axis ellipsoidal reflector is thus an ideal geometry for maximizing collecting area, combined with minimal deployment requirement.

ACKNOWLEDGMENTS

We are very grateful to Dustin Crumb of ATK Space for very efficiently making many drawings of CALISTO, carrying out calculations, and supporting this effort in many other ways. We thank David Frayer for carrying out calculations of the confusion limit for *CALISTO*. This work has made use of NASA's Astrophysics Data System.

REFERENCES

1. M. Werner, G. Fazio, G. Rieke, T. L. Roellig, & D .M. Watson, "First Fruits of the *Spitzer Space Telescope*: Galactic and Solar System Studies," *Ann. Rev. Astron. Astrophys.* **44**, pp. 269–321, 2006.
2. D. Lester *et al.*, "Science Promise and Conceptual Mission Design Study for SAFIR - the Single Aperture Far Infrared Observatory. Final Report NASA NRA-03-OSS-01_VM Call for Mission Concepts: Space Science Vision Missions", 2005.
3. P. Goldsmith, B. Khayatian, M. Bradford, M. Dragovan, D. Hoppe, W. Imbriale, R. Lee, C. Paine, P. Turner, H. Yorke, & J. Zmuidzinas, "Analysis of the Optical Design for the SAFIR Telescope," *Proc. SPIE*, **6265**, pp. 6265A-3–6265A-9, 2006.

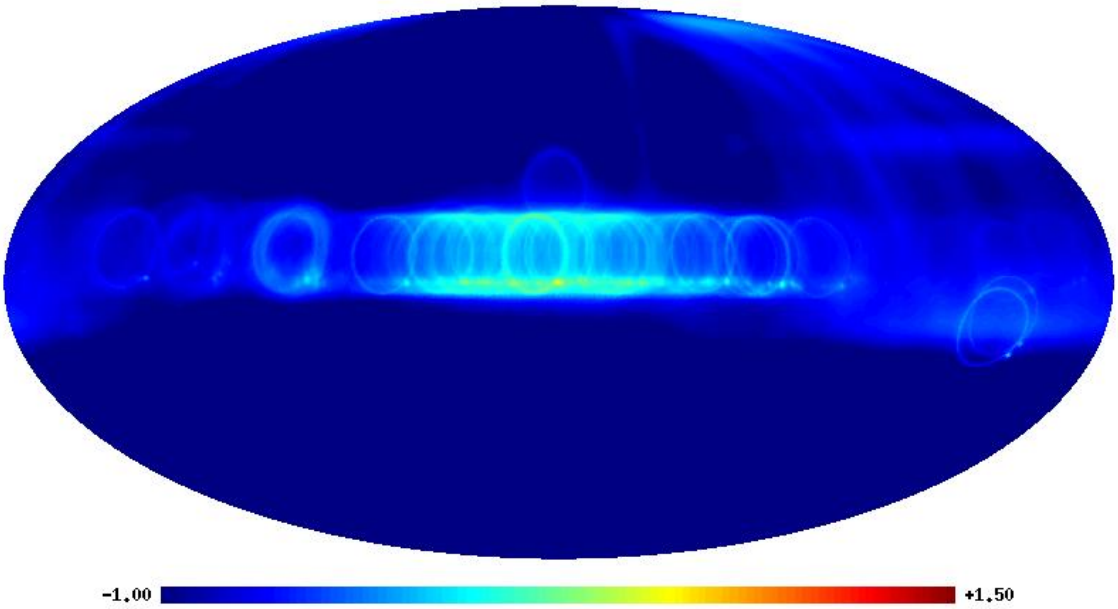

Figure 10. Sky brightness at 100 μm wavelength as measured with the off–axis *CALISTO* configuration including the cold stop. The spacecraft has been rotated approximately 180° relative to Fig. 9. The orientation of the secondary edge diffraction features has rotated in consequence. The response of the main beam and close–in primary reflector diffraction sidelobes has been supressed. The scale is $log_{10}(I_{100\mu m}/MJysr^{-1})$.

4. P. Goldsmith, B. Khayatian, C. M. Bradford, M. Dragovan, W. Imbriale, R. Lee, H. Yorke, & J. Zmuidzinas, "Optical Performance of Designs for a Large Aperture Far-Infrared Telescope," *Bull. Amer. Astr. Soc.* **38**, p. 969, 2006.
5. H. W. Yorke, P. F. Goldsmith, C. M. Bradford, J. Zmuidinas, C. Paine, M. Dragovan, C. M. Satter, A. E. Nash III, R. A. Lee, B. Khayatian, A. R. Girerd, & S. J. MacLellan, "CALISTO: A Far-Infrared Observatory for the Next Decade," *Bull. Amer. Astr. Soc.***38**, p. 1130, 2006.
6. J. Zmuidzinas, "Thermal Noise and Correlations in Photon Detection," *Appl. Optics*, **42**, pp. 4989–5008, 2003.
7. D. J. Benford, M. J. Amato, J. C. Mather, S. H. Moseley Jr., & D. T. Leisawitz, "Mission Concept for the Single Aperture Far–Infrared(SAFIR) Observatory," *Astrophys. Space Sci.* **294**, pp. 177-212, 2004.
8. D. J. Schlegel, D. P. Finkbeiner, & M. Davis, "Maps of Dust Infrared Emission for Use in Estimation of Reddening and Cosmic Microwave Background Foregrounds," *Astrophys. J.*, **500**, pp. 525–553, 1998.
9. Wandelt, B.D. & Górski, K.M. 2001, "Fast Convolution on the Sphere," *Phys. Rev. D.*, **63**, pp. 123002-1 – 123002-6.
10. T. Kelsall, J. L. Weiland, B. A. Franz, W. T. Reach, R. G. Arendt, E. Dwek, H. T. Freudenreich, M. G. Hauser, S. H. Moseley, N. P. Odegard & E. L. Wright, "The COBE Diffuse Infrared Background Experiment Search for the Cosmic Infrared Background. I. Model of the Interplanetary Dust Cloud," *Astrophys. J.*, **508**, pp. 44–73, 1998.

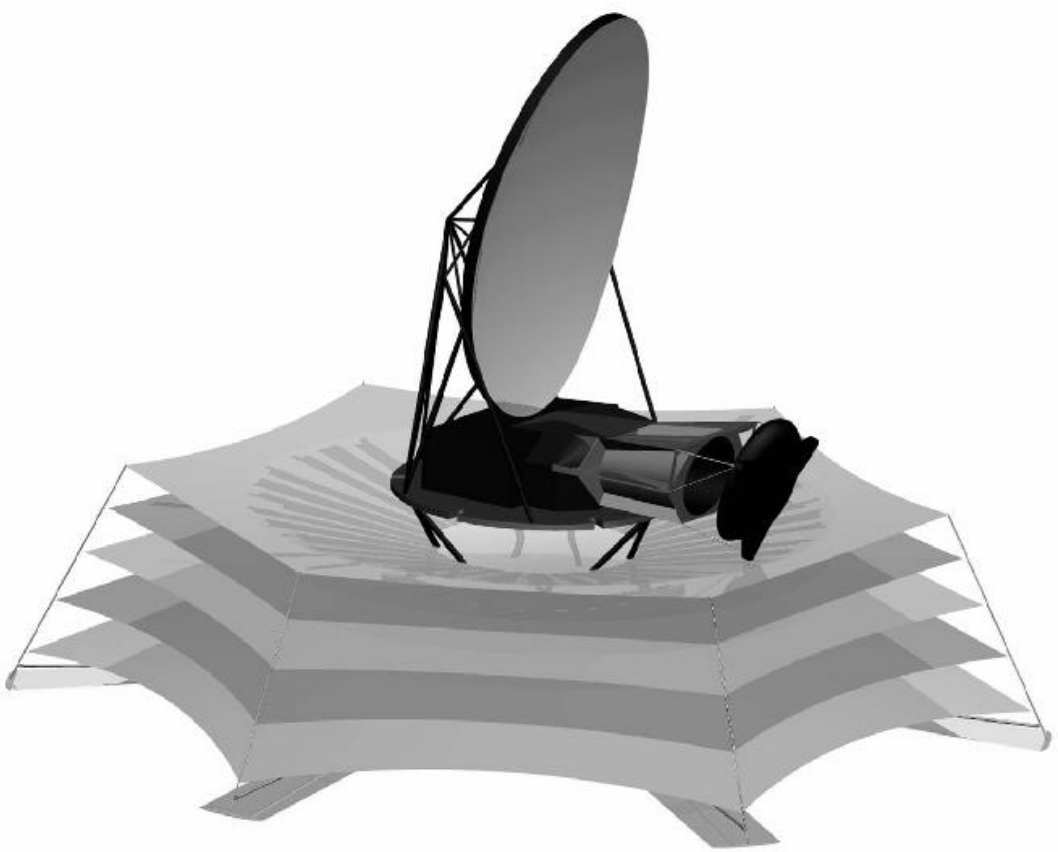

Figure 11. View of CALISTO spacecraft showing primary and secondary reflectors, cold stop, and instrument enclosure(below the primary reflector), all cooled to 4 K. The projected dimensions of the primary reflector are 4 m by 6 m. The multilayer V–groove sunshade is also shown.

Parameter	Value
Orbit	L2 Halo
Mission Duration	5 yr plus 4 month cruise
Launch Trajectory	2 earth flybys plus 1 lunar flyby
Launch Mass	3000 kg
Launch Vehicle	Atlas V 511
Instruments	30 μm to 300 μm cameras and low–res. spectrometers
Instrument & Spacecraft Power	725 W
Cooler Power	1200 W
Solar Cell Area	14 m^2
Beam size	1.2″ at 30 μm; 12″ at 300 μm
Pointing Control	0.4″
Data Rate	10 mb/s
Primary Reflector Dimensions	4 m x 6 m
Telescope Type	Unblocked Aplanatic Gregorian
Telescope Projected Physical Area	18.8 m^2
Reflector & Structure Material	SiC
Cost	$1 Billion – $1.5 Billion

Figure 12. Selected parameters for *CALISTO* spacecraft and mission. The values here are representative of the range in the options that have been considered.